**Proceedings of ASME Turbo Expo 2011**
**GT2011**
**June 6-10, 2011, Vancouver, British Columbia, Canada**

**GT2011-45505**

# AEROELASTIC ANALYSIS OF BLADES CASCADES THROUGH AERODYNAMIC REDUCED-ORDER MODELING

**Davide Finamore**
Department of Mechanical and Industrial Engineering
University Roma Tre
Rome, Italy

**Fred Nitzsche**
Department of Mechanical and Aerospace Engineering
Carleton University
Ottawa, ON, Canada

**Massimo Gennaretti**
Department of Mechanical and Industrial Engineering
University Roma Tre
Rome, Italy

## ABSTRACT

*An aerodynamic Reduced-Order Model (ROM) is introduced to describe the aeroelastic behavior of a blade cascade of a turbomachine. This is obtained coupling an aerodynamic model with a semi-rigid 2D model for the description of the structure dynamics. The advantages of using an aerodynamic reduced-order model concern the high computational efficiency compared to the direct use of a CFD code, and the applicability of control laws to reduce, for instance, blades vibrations. ROMs are identified from both an analytical aerodynamic model and a numerical CFD solver. The aeroelastic stability of a blade cascade is examined with the presence or not of mistuning.*

## NOMENCLATURE

$b$ Semi-chord.
$c$ Blade chord.
$C_{lh}, C_{l\alpha}$ Non-dimensional lift coefficients due to bending and torsional motions, respectively.
$C_{mh}, C_{m\alpha}$ Non-dimensional moment coefficients due to bending and torsional motions, respectively.
$h_{ar}$ Amplitude of bending deflection of a blade in $r$th mode of tuned rotor.
$h_n$ Amplitude of bending deflection of the $n$th blade.
$i$ $= \sqrt{-1}$
$J_E$ Mass moment of inertia about the elastic axis per unit span.
$k_h, k_\alpha$ Bending and torsional stiffness, respectively.
$m$ Mass per unit span of the blades.
$n$ Blade Index.
$N$ Number of blades in the cascade.
$r$ Aerodynamic mode index.
$r_\alpha^2$ Radius of giration of the blade section $(= \frac{J_E}{m\, b^2})$.
$s$ Laplace variable.
$t$ Time.
$U_\infty$ Freestream velocity.
$\hat{U}$ Reduced velocity $(= \frac{U_\infty}{b\omega_\alpha})$.
$\mathtt{X}, \mathtt{Y}$ Vectors of physical and aerodynamic variables, respectively.
$\mathtt{z}$ Vector of the system variables in the state-space form.
$\alpha_n$ Torsional amplitude of the $n$th blade.
$\alpha_{ar}$ Torsional amplitude of a blade in $r$th mode of tuned rotor.
$\beta_r$ Interblade phase angle in $r$th mode.
$\lambda$ Reduced frequency $(= \frac{\omega c}{U_\infty})$
$\mu$ Mass ratio of the blade $(= \frac{m}{\pi\rho b^2})$.
$\xi$ Stagger angle.
$\xi_E$ Location of the elastic axis $(= \frac{x_E}{b})$.
$\xi_G$ Location of the center of mass $(= \frac{x_G}{b})$.
$\rho$ Freestream density.
$\omega$ Motion frequency of the system.
$\hat{\omega}$ Non-dimensional frequency $(= \frac{\omega}{\omega_\alpha})$.
$\omega_\alpha$ Torsional natural frequency of the blades.
$\omega_h$ Bending natural frequency of the blades.
$\Omega$ Bending-torsion frequency ratio $(= \frac{\omega_h}{\omega_\alpha})$.

## INTRODUCTION

The continuing demand for increased performance in gas turbine engines makes dynamics behavior problems in the various components worse (this is particularly true for the blading). These problems are generally classified into the categories of either flutter or forced response. Historically, the complexity of the flowfield in turbomachines required the application of empirical flutter and forced-response analyses in the design process. However, such empirical correlations have proven to be inadequate when extrapolated beyond past experiences, [1, 2]. According to the development of computing resources in the past 30 years, the use of CFD codes has been introduced to study these problems. However, although a CFD simulation may yield a detailed time history of all problem variables, it is not suitable for spectral aeroelastic analysis and aeroservoelastic applications. An accurate prediction of the flowfield and the corresponding aerodynamic loads still requires a significant computational effort. These limitations suggest the introduction of aerodynamic lower-order models to be coupled with structural dynamics.

A Reduced-Order-Model (ROM) can be defined as a model which, starting from the data provided by an accurate solution tool dealing with a high number of degrees of freedom, is able to simulate satisfactorily the evolution a physical process through a (significantly) lower number of degrees of freedom. Thus, it allows the numerical analysis of complex physical phenomena at low computational costs. In the past years, a lot of research effort has been spent in developing Reduced-Order Models of unsteady aerodynamics of blade cascades for turbomachinery applications. Among them, Ref. [3] proposes a Proper Orthogonal Decomposition (POD) to obtain the ROM of an unsteady, frequency-domain, inviscid-viscous interaction flow solver, Ref. [4] applies an Arnoldi approach to determine the aerodynamic ROM from the linearized, state-space form of a solver based on the Euler equations for unsteady, two-dimensional flows of an inviscid compressible fluid, while Ref. [5] proposes an eigenmode-based reduction model, known as System Equivalent Reduction Expansion Process (SEREP), applied to the analytical incompressible aerodynamic solution model presented in Ref. [6].

Here, an aerodynamic ROM aimed at state-space aeroelastic modeling of blade cascades is proposed. It is not based on the reduction of the degrees of freedom involved in the aerodynamic solver, but rather consists of the rational matrix approximation of the aerodynamic transfer functions relating blade loads to blade degrees of freedom. Hence, it allows the expression of the aeroelastic equations in state-space form, which is particularly convenient for the eigenvalue stability analysis, as well as for aeroservoelastic applications. The aerodynamic ROM proposed may be applied to 2D and 3D configurations, depending on the aerodynamic tool available for the identification of the transfer functions between the degrees of freedom of the problem examined and the corresponding generalized forces. In the past, this approach has been successfully applied to describe the unsteady aerodynamics of wing-tail configurations and helicopter rotors (see, for instance, Ref. [7]).

In the numerical investigation, the rational matrix approximation of aerodynamic transfer functions will be applied to obtain ROMs of the incompressible, unsteady aerodynamics of blade cascades based both on analytical solutions [6] and on the predictions from the well validated commercial CFD code, ANSYS CFX®, and the correlations between the two resulting models will be discussed (validation of the results from ANSYS CFX® is well beyond the scope of this paper). The suitability of the proposed ROM for aeroelastic analysis will be proven by examining the stability of tuned and mistuned blade cascades.

## 1 THE BLADE CASCADE MODEL

In order to perform the aeroelastic analysis of a realistic 3D blade assembly as shown in Figure 1, a model is derived as a 2D cascade of infinite airfoils (Figure 2) representing the blade sections at a radial position, $R$.

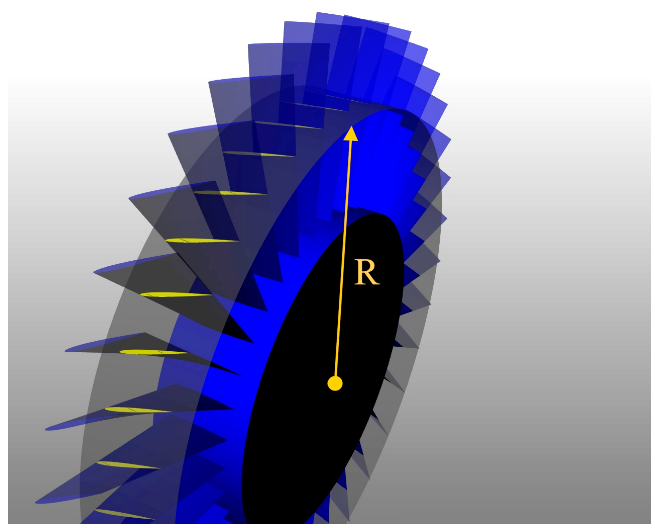


**FIGURE 1**. The 3D blade assembly

The stagger angle, $\xi$ indicates the inclination of the blade sections with respect to the axial direction. The upstream velocity, $U_\infty$ is parallel to the chord of the blades and its magnitude coincides with the magnitude of the vectorial summation of the axial velocity and the tangential velocity due to the rotating motion. The bending and torsion deformations of the blades are represented by the displacement normal to the blade chord, $h_n$ and the rotation, $\alpha_n$ about its elastic axis. The disk is assumed to be rigid, thus implying that the blades are structurally uncoupled. Concerning to the blades structural properties, it is possible

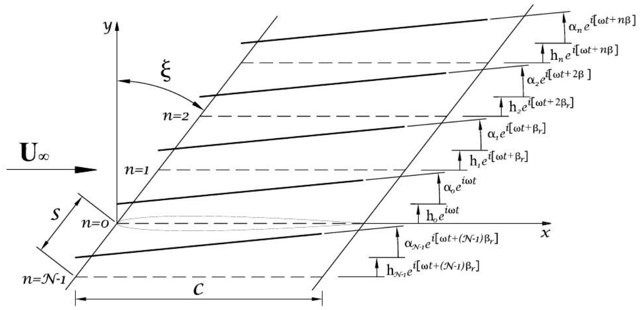


**FIGURE 2**. The 2D blade cascade model

to distinguish between two cases: tuned and mistuned blade cascades.

### 1.1 TUNED CASCADE

A tuned bladed disk is considered as a periodic structure in which all the blades are structurally identical. For aeroelastic modeling purposes, the motion of each blade is assumed to be harmonic with constant amplitude and an interblade phase angle, $\beta_r$, between adjacent blades. The values of the interblade phase angles are limited using Lane's assumption [8] to $N$ discrete values, $\beta_r = 2\pi r/N$, where $r = 0, 1, ..., N-1$ ($N$ denotes the number of blades in the cascade). This means that the interblade phase angle becomes the aerodynamic mode index. It can be demonstrated that for a tuned cascade, cascade (or aerodynamic) modes with different interblade phase angles are uncoupled [8]. Hence, as stated in Ref. [9], the bending-torsion motion of the $n$-th blade due to the $r$-th aerodynamic mode can be represented in the following traveling waves representation:

$$\left\{ \begin{array}{c} \tilde{h}_n \\ \tilde{\alpha}_n \end{array} \right\} e^{i\omega t} = \left\{ \begin{array}{c} \tilde{h}_{ar} \\ \tilde{\alpha}_{ar} \end{array} \right\} e^{i(\omega t + \beta_r n)} \tag{1}$$

where $n = 0, 1, ..., N-1$. The variables $\tilde{h}_n, \tilde{\alpha}_n$ represent the amplitudes of the motion of the $n$-th blade, while $\tilde{h}_{ar}, \tilde{\alpha}_{ar}$ represent the amplitudes of the $r$-th aerodynamic mode. Therefore, in a tuned cascade if the motion of the reference blade ($n = 0$) is known the motion of the other blades can be also obtained using the interblade phase angle information($e^{i\beta_r n}$). Then, for a given aerodynamic mode, the flutter stability and the response problem concerning the reference blade is representative of the whole blade cascade.

### 1.2 MISTUNED CASCADE

Bladed wheels are generally designed to be a cyclically symmetric structure. In reality, however, due to casting process and machining tolerances, there are always random variations in geometry and material property among blades. This unavoidable phenomenon is called mistuning [10]. As a result, each blade has mass and natural frequencies of vibration different from those of the other blades. Since the cascade has a finite number of modes, and since each blade is different from the others, the motion of each blade can be viewed as a superposition of all possible traveling wave modes [9]:

$$\left\{ \begin{array}{c} \tilde{h}_n \\ \tilde{\alpha}_n \end{array} \right\} e^{i\omega t} = \sum_{r=0}^{N-1} \left\{ \begin{array}{c} \tilde{h}_{ar} \\ \tilde{\alpha}_{ar} \end{array} \right\} e^{i(\omega t + \beta_r n)} \tag{2}$$

Considering the whole blade cascade, Eq.(2) can be expressed in the matrix compact form:

$$\tilde{\mathtt{X}} e^{i\omega t} = \mathtt{E} \tilde{\mathtt{Y}} e^{i\omega t} \tag{3}$$

where the vector $\tilde{\mathtt{X}}$ collects the amplitudes of the mechanical degrees of freedom of the blades in the cascade, the vector $\tilde{\mathtt{Y}}$, collects the amplitudes of the aerodynamic modes (each representing a cascade motion with different interblade phase angles, *i.e.*, the amplitudes of the aerodynamic modes) and the matrix $\mathtt{E}$ gives the motion of each blade as the superposition of all aerodynamic modes.

## 2 AEROELASTIC EQUATIONS

As mentioned above, semi-rigid 2D blade models undergoing translations, $h_n(t)$ and rotations, $\alpha_n(t)$ are considered here. Bending and torsional stiffnesses are simulated by two springs with constants $k_h$ and $k_\alpha$, respectively (see Figure 3). Inertial centrifugal effects are assumed and included in the spring constants.

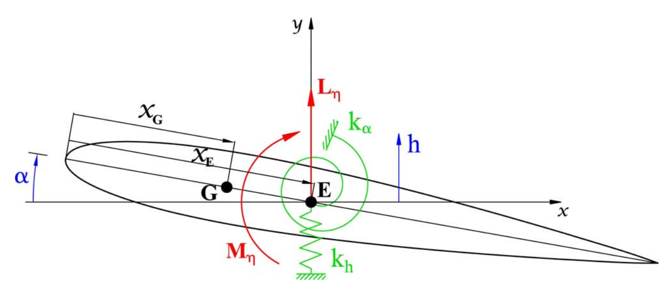


**FIGURE 3**. 2D representation of a cascade blade

Thus, following Ref. [9], the non-dimensional aeroelastic equations of motion of the $n$-th blade in the frequency domain are expressed as:

$$-\hat{\omega}^2 \left[ \begin{array}{cc} 1 & (\xi_G - \xi_E) \\ (\xi_G - \xi_E) & r_\alpha^2 \end{array} \right] \left\{ \begin{array}{c} \frac{\tilde{h}_n}{b} \\ \tilde{\alpha}_n \end{array} \right\} + \left[ \begin{array}{cc} \Omega^2 & 0 \\ 0 & r_\alpha^2 \end{array} \right] \left\{ \begin{array}{c} \frac{\tilde{h}_n}{b} \\ \tilde{\alpha}_n \end{array} \right\} = \left\{ \begin{array}{c} \tilde{L}_n \\ \tilde{M}_n \end{array} \right\}$$

or, in compact form,

$$-\hat{\omega}^2 \mathtt{M}_n \tilde{\mathtt{X}}_n + \mathtt{K}_n \tilde{\mathtt{X}}_n = \tilde{\mathtt{F}}_{a,n} \tag{4}$$

where the vector $\tilde{\mathtt{F}}_a$ denotes the contribution of the aerodynamic loads, which can be calculated using either an analytical model or a numerical (CFD) solver. In this section, the aeroelastic system is derived by using an analytical aerodynamic model, while the use of a numerical solver is presented in Section 4. Here, the analytical model applied is that presented in Ref. [6] for incompressible, unsteady flows around an airfoil cascade. Akin to the blade cascade motion, the aerodynamic loads are described as a superposition of the aerodynamic modes [9] (see Appendix A and Ref. [6], for details)

$$\tilde{\mathtt{F}}_a = \frac{\hat{U}^2}{\mu} \left\{ \begin{array}{l} \sum_{r=0}^{N-1} \left[ C_{lh}(\lambda,\beta_r) \frac{\tilde{h}_{ar}}{b} + C_{l\alpha}(\lambda,\beta_r)\tilde{\alpha}_{ar} \right] e^{i\beta_r n} \\ \sum_{r=0}^{N-1} \left[ C_{mh}(\lambda,\beta_r) \frac{\tilde{h}_{ar}}{b} + C_{m\alpha}(\lambda,\beta_r)\tilde{\alpha}_{ar} \right] e^{i\beta_r n} \end{array} \right\}$$

Therefore, the non-dimensional aerodynamic load vector for the entire cascade is given by:

$$\tilde{\mathtt{F}}_a = \frac{\hat{U}^2}{\mu} \mathtt{EL}(\lambda) \tilde{\mathtt{Y}} \tag{5}$$

where the matrix $\mathtt{E}$ is identical to that in Eq. (3), while $\mathtt{L}$ is a block diagonal matrix in which each $r$-th block, $\mathtt{L}_r$ is defined as (see also Appendix A):

$$\mathtt{L}_r = \begin{bmatrix} C_{lh}(\beta_r,\lambda) & C_{l\alpha}(\beta_r,\lambda) \\ C_{mh}(\beta_r,\lambda) & C_{m\alpha}(\beta_r,\lambda) \end{bmatrix}$$

Then, according to Eq.(4), the equations of motion for the whole blade cascade can be derived. Specifically, recalling Eq.(3), these equations can be written either in terms of aerodynamic mode variables, $\mathtt{Y}$,

$$-\hat{\omega}^2 \mathtt{E}^{-1}\mathtt{ME}\tilde{\mathtt{Y}} + \mathtt{E}^{-1}\mathtt{KE}\tilde{\mathtt{Y}} = \frac{\hat{U}^2}{\mu} \mathtt{L}\tilde{\mathtt{Y}} \tag{6}$$

or in terms of physical displacements, $\mathtt{X}$,

$$-\hat{\omega}^2 \mathtt{M}\tilde{\mathtt{X}} + \mathtt{K}\tilde{\mathtt{X}} = \frac{\hat{U}^2}{\mu} \mathtt{ELE}^{-1}\tilde{\mathtt{X}} \tag{7}$$

where $\mathtt{M}$ and $\mathtt{K}$ are the mass and stiffness matrices of the whole blade cascade, respectively. Since the disk is assumed to be rigid, the cascade mass and stiffness matrices are block diagonal. In the tuned case, the blocks are equal and it is possible to prove that $\mathtt{E}^{-1}\mathtt{ME} = \mathtt{M}$ and $\mathtt{E}^{-1}\mathtt{KE} = \mathtt{K}$. Hence, as stated by Lane [8], the use of the aerodynamic modes uncouples the equations (see Eq. (6)) and the system stability may be examined considering a sequence of $N$ problems, each one concerning one aerodynamic mode. In a mistuned situation, the matrices $\mathtt{M}$ and $\mathtt{K}$ are still block diagonal, but the blocks are not equal. This means that in Eq. (6) the structural matrices, $\mathtt{E}^{-1}\mathtt{ME}$ and $\mathtt{E}^{-1}\mathtt{KE}$ are no longer block diagonal. Thus, only the aerodynamic contributions are still uncoupled. Therefore, for a mistuned bladed disk, the analysis of aeroelastic stability in terms of aerodynamic modes has to be carried out considering larger $2N \times 2N$ matrices representing the blade cascade as a whole.

In Eq.(7) the aeroelastic equations are expressed in terms of physical variables, $\tilde{\mathtt{X}}$. In this representation, while the structural matrices remain uncoupled both for tuned and mistuned cascades, the aerodynamics always couples the dynamics of different blades. This is due to the aerodynamic matrix $\mathtt{ELE}^{-1}$, which is not block diagonal. A non-zero aerodynamic contribution of all physical degrees of freedom on any generalized aerodynamic force appearing in the aeroelastic equations is present. Therefore, in this case, the stability analysis requires all the blades to be examined as a whole.

The stability margins of the aeroelastic system described by Eqs. (6) and (7), both in the tuned and in the mistuned case may be estimated through the V-g method.

## 3 AERODYNAMIC REDUCED ORDER MODEL

Analytical unsteady aerodynamic models yield transcendent frequency response functions relating loads to kinematic variables. As shown (for instance) in Refs. [6, 11, 12], this occurs because of the influence of the convected wake vorticity, from which time-delayed terms appear. These aerodynamic models, when coupled with structural dynamics, yield aeroelastic systems not suitable for aeroservoelastic applications, from which only an estimation of the stability margins through the V-g method may be obtained. In order to determine the complete aeroelastic response spectra and to express the aeroelastic equations in a state-space form suitable for aeroservoelastic applications (*i.e.,* in a form that is suitable to design stability augmentation control laws) a finite-state (or reduced-order) model of the aerodynamic contribution has to be introduced.

In this work, considering the following relationship between aerodynamic loads, $\tilde{\mathtt{F}}_a$, and physical degrees of freedom, $\tilde{\mathtt{X}}$,

$$\tilde{\mathtt{F}}_a = \frac{\hat{U}^2}{\mu} \mathtt{A}_B(\lambda)\, \tilde{\mathtt{X}} \tag{8}$$

where $\mathtt{A}_B = \mathtt{ELE}^{-1}$ (see Eq. (7)), the aerodynamic ROM is obtained through the rational matrix approximation of the aerodynamic matrix $\mathtt{A}_B$, as a function of $\lambda$ [7]. As the frequency tends to infinity the behavior of the imaginary parts of the transfer functions in $\mathtt{A}_B$ is asymptotically linear, whereas the behavior of their real part is asymptotically quadratic. Hence, the rational matrix approximation introduced has the following form

$$\mathtt{A}_B(s) \approx s^2\mathtt{A}_2 + s\mathtt{A}_1 + \mathtt{A}_0 + \mathtt{C}\,(s\mathtt{I} - \mathtt{A})^{-1}\,\mathtt{B}$$

where $s = g + i\lambda$. The matrices $\mathtt{A}_2$, $\mathtt{A}_1$, $\mathtt{A}_0$, $\mathtt{B}$, $\mathtt{C}$ and $\mathtt{A}$ are real and fully populated, and are identified by a least-square approximation technique (see Appendix B and Ref. [7] for details). It is worth noting that the proposed approach deals with the transfer functions of the blade physical variables, in that yielding a ROM conveniently expressed in terms of real-coefficient matrices. This would not be possible if the transfer functions of the aerodynamic mode variables were considered because in general, they are complex even at zero frequency [6].

Next, coupling the equation above with Eq. (7), and transforming back into the time domain, the following aeroelastic system is obtained

$$\begin{cases} \frac{\hat{U}^2}{4}\mathtt{M}\ddot{\mathtt{X}} + \mathtt{K}\mathtt{X} = \frac{\hat{U}^2}{\mu}\left(\mathtt{A}_2\ddot{\mathtt{X}} + \mathtt{A}_1\dot{\mathtt{X}} + \mathtt{A}_0\mathtt{X} + \mathtt{C}\mathtt{r}\right) \\ \dot{\mathtt{r}} = \mathtt{A}\mathtt{r} + \mathtt{B}\mathtt{X} \end{cases}$$

where $\mathtt{r}$ is the vector of the additional aerodynamic states (related to the convection of the wake vorticity), and $\dot{()}$ denotes derivative with respect to nondimensional time, $\tau = tU_\infty/c$. The equations above may be recast in state-space form, which may be conveniently applied for the evaluation of complete aeroelastic spectrum, for control design purposes and for the determination of responses to external inputs.

## 4 AERODYNAMICS IDENTIFICATION VIA CFD CODE

In the analytical aerodynamic model some assumptions have been introduced in order to simplify the problem. For instance, in Section 3 the flow has been considered to be inviscid and incompressible. A more accurate aerodynamic solution including viscosity and compressibility effects, along with realistic blades (airfoil) geometry, may be obtained via a CFD solver. Here, the commercial CFD code ANSYS CFX v12.1® has been applied to identify the aerodynamic transfer functions matrix, $\mathtt{A}_B$, from which, in turn, an aerodynamic ROM that is more accurate than the one based on the analytical aerodynamic model has been determined.

The identification of matrix $\mathtt{A}_B$ has been carried out following two approaches: one based on aerodynamic modes and one based on physical modes. In the aerodynamic modes approach (AMA), the transfer functions matrix, $\mathtt{EL}$ appearing in Eq. (5) is first identified imposing as input the motion of all blades according to each aerodynamic mode (*i.e.,* following each interblade phase angle), and then the post-multiplication with $\mathtt{E}^{-1}$ is applied. In the physical modes approach (PMA), the transfer functions matrix, $\mathtt{A}_B$ is directly identified from a sequence of solutions, each concerning the loads produced on all blades by the forced motion of one single blade in the cascade.

In both approaches, in order to evaluate the rational matrix approximation of $\mathtt{A}_B$, it is necessary to obtain the sampling of the aerodynamic transfer functions in the frequency range of interest. The evaluation of the transfer functions of the linearized aerodynamics is determined from the computation of the responses due to a small-amplitude, harmonic blade motion expressed as follows

$$h_n = A_h \sum_{j=1}^{N_f} sin(\omega_j t) \qquad \alpha_n = A_\alpha \sum_{j=1}^{N_f} sin(\omega_j t)$$

where $N_f$ is the number of harmonics included in the motion, and $A_h$, $A_\alpha$ are the small plunging and pitching amplitudes, respectively. Specifically, the linearized aerodynamic transfer functions are determined from the evaluation of amplitude and phase of the corresponding harmonics of the computed loads. Note that the inclusion of multiple harmonics in the input blade motion reduces the number of aerodynamic solutions to be computed (it becomes significantly lower than the number of sampling frequencies). However, the number of frequencies that may be examined in the same solution is in practice limited by the mesh deformation model refinement.

## 5 NUMERICAL RESULTS

The aerodynamic ROM presented above has been applied for the aeroelastic analysis of a blade cascade. Both a ROM based on an analytical aerodynamic model and a ROM based on the results from a numerical solver have been used. In order to limit the computational cost (but without affecting the generality of the results obtained), a cascade with a small number of blades has been considered. The geometric and structural parameters of the blade cascade examined are given in Table 1.

| | | | |
|---|---|---|---|
| $N = 8$ | $s/c = 2$ | $\xi = 60^o$ | $\xi_E = 1$ |
| $\mu = 100$ | $\xi_G = 1$ | $r_\alpha = 0.5774$ | $\Omega = 0.1 \rightarrow 1$ |

**TABLE 1**. Parameters of airfoil cascade.

## 5.1 IDENTIFICATION FROM ANALYTICAL MODEL

First, results from the ROM based on the analytical aerodynamic model are presented. For the cascade considered, the rational approximation has been obtained introducing 640 aerodynamic states. As an example, Figure (4) shows the real part of the transfer function $\mathbb{A}_{B31}$ evaluated analytically and approximated through the rational expression. The agreement between the two curves is excellent and a similar quality of the approximation might be shown for all transfer functions in the matrix $\mathbb{A}_B$. Next, the aerodynamic ROM has been applied for the flutter analysis of the cascade, in the range $0 \leq \Omega \leq 1$, considering both tuned and mistuned cases. Note that although mistuning is of random nature, for the purposes of this work a deterministic mistuning is considered. Specifically, a 3% variation of the natural bending and torsion frequencies has been assumed between two adjacent blades (with positive and negative signs, alternatively). Figure (5) compares the flutter velocities determined using the present aerodynamic ROM with those predicted by the application of the V-g method to the aeroelastic system directly obtained from Ref. [6]. From the observation of the quality of the rational approximation in Figure (4) for both the tuned and mistuned configuration, the flutter predictions from the aerodynamic ROM are in excellent agreement with those from the exact aerodynamic theory. This result validates the ROM introduced.

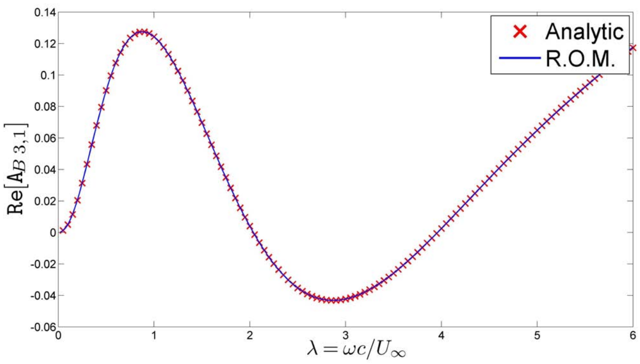


**FIGURE 4**. Real part of the transfer function $\mathbb{A}_{B31}$.

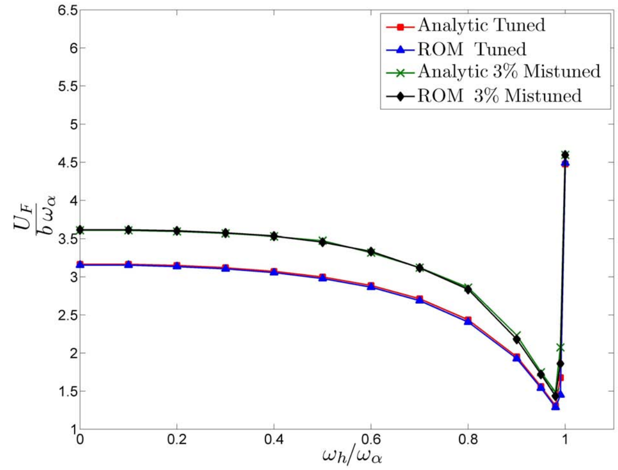


**FIGURE 5**. Cascade flutter velocity vs $\Omega$.

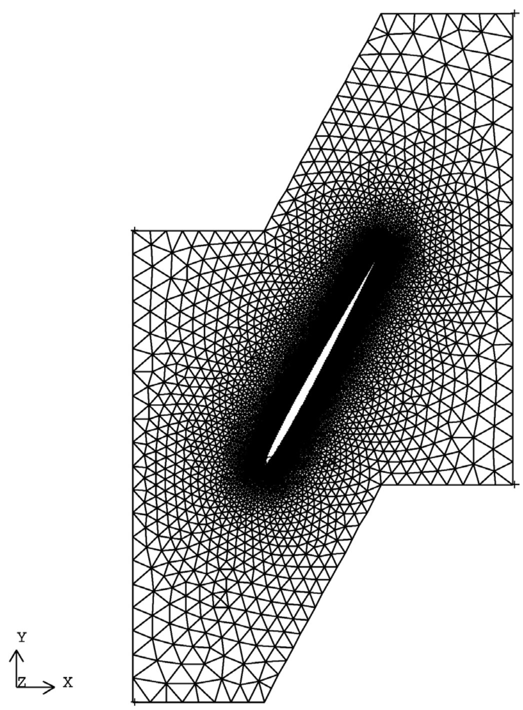


**FIGURE 6**. Mesh structure for one blade passage.

## 5.2 IDENTIFICATION FROM NUMERICAL MODEL

The geometry of the airfoil cascade in Table 1 and corresponding meshes have been created using the software ANSYS Gambit®. As stated in Ref. [13], computations are in general made using a number of blade passages equal to the number of the blades in the cascade. Periodic boundary conditions are applied at the upper and lower boundaries of the cascade. However, there are some situations in which it is possible to reduce the number of blade passages used in the calculations. For the steady flow through a stationary cascade, blade-to-blade periodicity of flow variables occurs. Hence, only a single blade passage is used in computations; periodic conditions are imposed at the upper and lower boundaries of the blade passage. The flowfield is simply reproduced for the remaining blade passages. For unsteady flows in which all the blades have the same periodic motion (zero interblade phase angle), the same situation occurs.

Then, only a single blade passage can be used. For periodic motion with non-zero interblade phase angle, it is occasionally possible to reduce the number of the blade passages used in the calculations. This depends on the value of the interblade phase angle. For instance, computations with the phase angle $\beta = 180°$, can be made through two passages, computations with $\beta = 120°$ or $240°$, can be made in three passages, etc. Therefore, in this contest four meshes have been created (see Table 2).

| $N_{Pass}$ | $\beta$ | Elements |
|---|---|---|
| 1 | $0^o$ | $35K$ |
| 2 | $180^o$ | $70K$ |
| 4 | $90^o, 270^o$ | $140K$ |
| 8 | $45^o, 135^o, 225^o, 315^o$ | $280K$ |

**TABLE 2**. Mesh parameters

The meshes have been imported in ANSYS CFX® where the boundary conditions, the blades motion, and the simulation parameters have been imposed. Next, solutions in the time domain, following both aerodynamic and physical modes approaches, have been determined. Then, inputs and outputs from the code have been transformed in the frequency domain and the aerodynamic transfer functions matrix was identified.

By comparing the results obtained following the two approaches, it can be noted that some transfer functions obtained via the physical modes approach (PMA) were not regular (see Figure (7)). This occurs because using this approach as only one

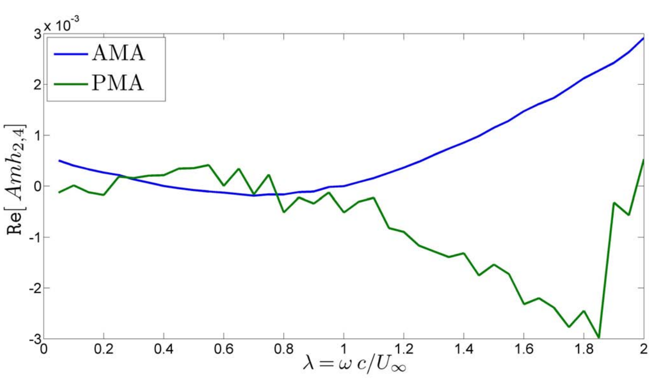


**FIGURE 7**. Real part of a transfer function from aerodynamic and physical modes approaches.

blade is moved the CFD code is not able to capture accurately all small interaction effects on adjacent blades. In particular, for the meshes applied, only the influence of one blade onto the two adjacent blades can be captured with a good level of accuracy. This result suggests that the aerodynamic modes approach (AMA) allows meshes with less elements and less blade passages, optimizing the computational time. However, the drawback of this approach lies on the high number of computations to be carried out. Indeed, the AMA requires a number of simulations equal to the number of blades multiplied by the number of degrees of freedom, while the PMA would require only one simulation per degree of freedom (but with a much finer computational grid).

### 5.3 COMPARISON BETWEEN ANALYTICAL AND NUMERICAL MODEL

Next, a comparison between transfer functions obtained from CFX using the two methods of identification mentioned above (AMA and PMA) and those obtained by the analytic formulation is presented. Figure 8 shows the real and imaginary

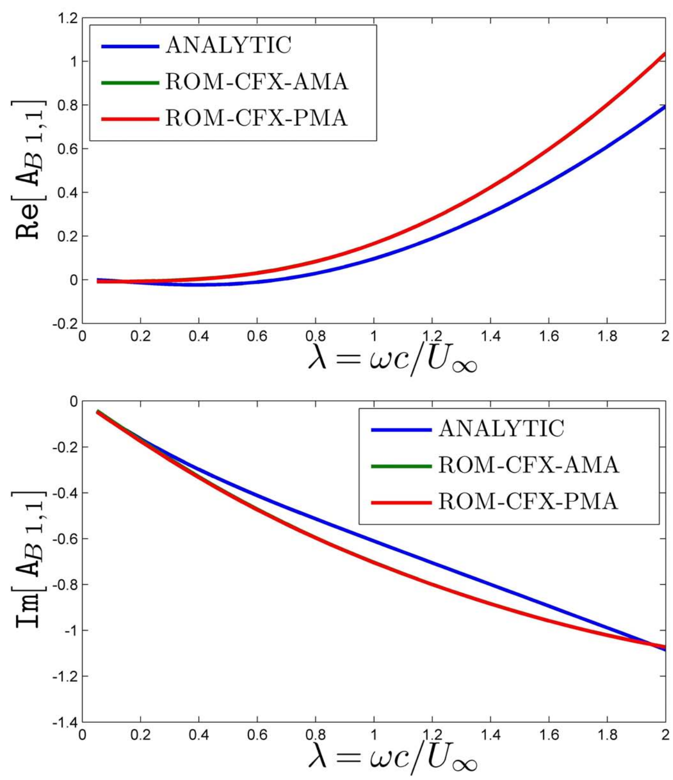


**FIGURE 8**. Real and imaginary parts of the transfer function relating lift and bending of the same blade.

parts of the transfer function relating lift and bending of the same blade as given by CFX using AMA and PMA, along with that obtained from Ref. [6]. It presents a good correlation between numerical and theoretical results and a perfect agreement between the AMA and PMA results. However, as a transfer function block-matrix gets farther from the main diagonal, because it represents the result of interaction aerodynamic effects, the differences between numerical predictions and analytical results increase, as well as the difference between the identifications through AMA and PMA. This is demonstrated, for instance, in Figure (9), which depicts the real and imaginary parts of the transfer function relating lift and bending of two adjacent blades. Correlations worsen for farther blades.

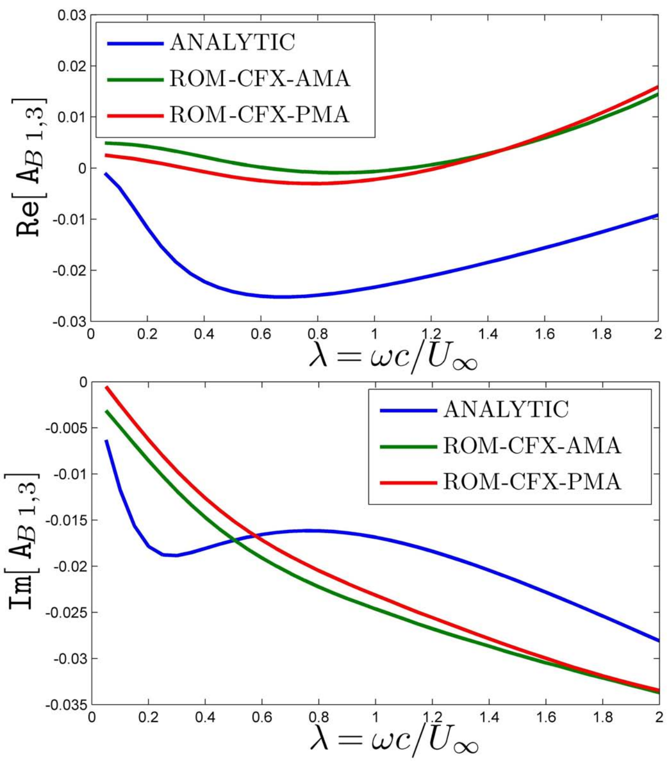


**FIGURE 9**. Real and imaginary parts of the transfer function relating lift and bending of two adjacent blades.

The rational matrix approximation of the transfer functions matrices obtained from the two numerical identification approaches has been carried out. This approximation reduces the states of the system from $2.1 \cdot 10^6$ to 992, following AMA, and to 616 following PMA. In both cases the accuracy of the approximated transfer functions is good and comparable to the results from the analytical solver, as seen in Figure (4). Thus for any blade motion the ROM simulation predicts loads identical to those that would be given directly by the CFD tool. It has to be recalled that following the physical modes approach, only the transfer functions relating adjacent blades can be accurately captured and approximated. However, since the influence of the blades far from the reference is very small, it is interesting to investigate their influence on flutter analysis.

Figure (10) presents the airfoil cascade flutter velocity as a function of the frequency ratio, $\Omega$, as given by application of the analytical aerodynamic model, and aerodynamic ROMs determined from CFX through AMA and PMA. It shows that although neglecting the effects from the transfer functions far from the diagonal in the PMA, the numerical results determined from the latter approach and the AMA are in very good agreement. However, a relevant discrepancy between the flutter velocities obtained with the analytical model and those obtained using CFX can be noted. This difference is due to several reasons. Among them:

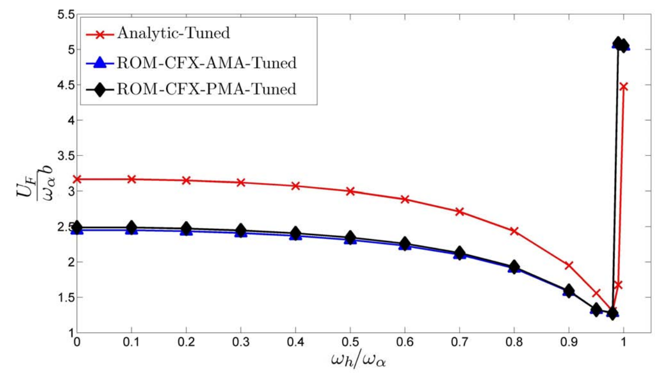


**FIGURE 10**. Cascade flutter velocity vs $\Omega$.

1. the analytical model is based on potential flow, while in CFX viscosity effects are taken into account;
2. the analytical model considers thin flat plates, while in CFX real airfoils are analyzed;
3. the analytic model introduces an infinite wake downstream the blades, while in CFX it is finite (in order to take into account the presence of a stator downstream, the wake has been assumed to be one-chord length).

On the other hand, CFD solvers may yield aerodynamic ROMs that take into account compressibility (transonic) effects, and the presence of stators upstream and downstream. Therefore, the use of an aerodynamic analytic model is suitable only for a qualitative aeroelastic analysis.

## 6 CONCLUSIONS

This work investigated the use of an aerodynamic ROM approach, obtained via rational matrix approximation of transfer functions, to study aeroelastic problems in axial-flow turbomachines. First, the aerodynamics of a rotor blade assembly has been modeled as an airfoil cascade, and an analytic formulation based on potential-flow assumption has been examined. Then, a CFD solver has been applied to evaluate more realistic aerodynamic transfer functions. For both models ROMs have been identified and coupled with a structural dynamic model to examine the aeroelastic behavior of the airfoil cascade in tuned and mistuned blade assemblies. The aerodynamic ROM presented has demonstrated to be a reliable tool for the aeroelastic analysis of airfoil cascades, as it predicts stability margins in perfect agreement with those given by the V-g method. In addition, advantages and disadvantages of the use of aerodynamic modes and physical modes in the identification of the transfer functions from the numerical solver have been discussed. Even for the simple airfoil cascade configuration assumed, the aerodynamic analytical model has shown some discrepancy in the flutter speed prediction with respect to the simulation obtained from the CFD solver, thus demonstrating to be a tool that is suitable only for a qualitative analysis of the aeroelastic behavior of a rotor blade assembly.

## APPENDIX A: THE ANALYTICAL AERODYNAMIC MODEL

The analytical aerodynamic model applied here is that presented in Ref. [6]. It has been developed to calculate the unsteady aerodynamic loads on a staggered airfoil cascade in incompressible potential flows. It is a linear model, valid for small perturbations around an equilibrium position (the freestream velocity is aligned with the airfoils). Each blade is considered as a straight thin plate without thickness and curvature, and is free to plunge and pitch. The flow is assumed to be attached to the airfoils. The harmonic response is given in terms of aerodynamic mode variables and the corresponding aerodynamic loads are expressed as

$$\begin{cases} \tilde{L} = \pi\rho U_\infty^2 b \left( C_{lh}(\lambda,\beta_r)\frac{\tilde{h}_{ar}}{b} + C_{l\alpha}(\lambda,\beta_r)\tilde{\alpha}_{ar} \right) \\ \tilde{M} = \pi\rho U_\infty^2 b^2 \left( C_{mh}(\lambda,\beta_r)\frac{\tilde{h}_{ar}}{b} + C_{m\alpha}(\lambda,\beta_r)\tilde{\alpha}_{ar} \right) \end{cases} \tag{9}$$

The coefficients $C_{lh}, C_{l\alpha}, C_{mh}$ and $C_{m\alpha}$ depend on the reduced frequency, $\lambda$, the interblade phase angle, $\beta_r$, the cascade geometry, and the location along the chord of the center of rotation of the blades. Note that, other aerodynamic models taking also into account flow compressibility effects have been developed in the past (see, for instance, Refs. [14]- [20]).

## APPENDIX B: MATRIX-FRACTION APPROXIMATION

In this appendix, the technique applied for the rational matrix approximation of the aerodynamic matrix, $\mathtt{A}_B$, is outlined. The first step in the approximation procedure starts from the observation that in the frequency domain, whatever the model used for the prediction of the aerodynamic loads, their asymptotic behaviors is quadratic, as the frequency tends to infinity. Therefore, following the formulation outlined in Ref. [21], the following form for the matrix-fraction approximation is considered

$$\begin{aligned} \mathtt{A}_B(s) \approx \hat{\mathtt{A}}_B(s) &= s^2\,\hat{\mathtt{A}}_2 + s\,\hat{\mathtt{A}}_1 + \hat{\mathtt{A}}_0 \\ &+ \left[\sum_{m=0}^{M} \mathtt{D}_m s^m\right]^{-1} \left[\sum_{m=0}^{M-1} \mathtt{R}_m s^m\right] \end{aligned} \tag{10}$$

The matrices $\hat{\mathtt{A}}_m, \mathtt{D}_m$ and $\mathtt{R}_m$ are real and fully populated (except for $\mathtt{D}_M$ that is chosen to be an identity matrix). They are determined by a least-square approximation technique along the imaginary axis. Specifically, the satisfaction of the following condition is required

$$\varepsilon^2 = \sum_j w_j\, \mathtt{Tr}\left[\mathtt{Z}^*(s_j)\,\mathtt{Z}(s_j)\right]\Big|_{s_j=ik_j} = \min$$

where $i=\sqrt{-1}$, $w_j$ denotes a suitable set of weights, and

$$\mathtt{Z}(s) := \left[\sum_{m=0}^{M} \mathtt{D}_m s^m\right]\left[s^2\,\hat{\mathtt{A}}_2 + s\,\hat{\mathtt{A}}_1 + \hat{\mathtt{A}}_0 - \mathtt{A}_B(s)\right] + \sum_{m=0}^{M-1} \mathtt{R}_m s^m$$

is a measure of the error $(\mathtt{A}_B - \hat{\mathtt{A}}_B)$.

Next, in order to use the matrix-fraction approximation to determine the time-domain relationship between the aerodynamic loads, $\mathtt{F}_a$, and the physical dofs, $\mathtt{X}$, Eq. (10) is recast in the following form

$$\hat{\mathtt{A}}_B(s) = s^2\,\hat{\mathtt{A}}_2 + s\,\hat{\mathtt{A}}_1 + \hat{\mathtt{A}}_0 + \hat{\mathtt{C}}\left[s\mathtt{I} - \hat{\mathtt{A}}\right]^{-1}\hat{\mathtt{B}} \tag{11}$$

where $\hat{\mathtt{C}}$ depends upon the $\mathtt{R}_m$'s, $\hat{\mathtt{A}}$ depends upon the $\mathtt{D}_m$'s, whereas $\hat{\mathtt{B}}^T = [\mathtt{I}, \mathtt{0}, \ldots, \mathtt{0}]$ (see Ref. [21] for details). Note that the accuracy of the approximation depends upon the number, $M$, of matrices used in the matrix-fraction term in Eq. (10). The appropriate value of $M$ depends upon the shape of the functions to be approximated. When a large number of poles (eigenvalues of the matrix $\hat{\mathtt{A}}$) are introduced in Eq. (11), some of them might be unstable: these are spurious (not physical) poles introduced by the interpolation procedure. In order to overcome this problem the iterative procedure of Ref. [21] is adopted. This consists of: (i) diagonalization (or block-diagonalization) of $\hat{\mathtt{A}}$, (ii) truncation of the unstable states (the matrix $\hat{\mathtt{A}}$ is modified into a smaller matrix $\mathtt{A}$), and (iii) application of an optimal fit iterative procedure to determine new matrices $\mathtt{A}_2, \mathtt{A}_1, \mathtt{A}_0, \mathtt{B}$, and $\mathtt{C}$ that replace, respectively, $\hat{\mathtt{A}}_2, \hat{\mathtt{A}}_1, \hat{\mathtt{A}}_0, \hat{\mathtt{B}}$, and $\hat{\mathtt{C}}$ (whereas $\mathtt{A}$ remains unchanged throughout the iteration). Hence, the matrix-fraction finite-state approximation assuring a good and stable fit of $\mathtt{A}_B(s)$ has the final form

$$\hat{\mathtt{A}}_B(s) = s^2\,\mathtt{A}_2 + s\,\mathtt{A}_1 + \mathtt{A}_0 + \mathtt{C}\,[s\,\mathtt{I} - \mathtt{A}]^{-1}\,\mathtt{B}$$

## REFERENCES


[1] Platzer, M.F. and Carta, F.O., (Eds.) AGARD Manual on Aeroelasticity in Axial-Flow Turbomachines, Volume 1, Unsteady Aerodynamics, AGARDograph No. 298, 1987.

[2] Platzer, M.F. and Carta, F.O., (Eds.) AGARD Manual on Aeroelasticity in Axial-Flow Turbomachines, Volume 2, Structural Dynamics and Aeroelasticity, AGARDograph No. 298, 1987.

[3] Epureanu, B.I., Hall, K.C. and Dowell, E.H., Reduced-Order Models of Unsteady Viscous Flow in Turbomachinery using Viscous-Inviscid Coupling, *Journal of Fluids and Structures*, 15, 255-273, 2001.

[4] Willcox, K., Peraire, J. and White, J., An Arnoldi approach for generation of reduced-order models for turbomachinery, *Journal of Computers & Fluids*, 31, 369-389, 2002.

[5] Sarkar, S. and Venkatraman, K., Model order reduction of unsteady flow past oscillating airfoil cascades, *Journal of Fluids and Structures*, 19, 239247, 2004.

[6] Whitehead, D.S., Force and Moment Coefficients for Vibrating Aerofoils in Cascade, *ARC R&M* 3254, London, 1960.

[7] Gennaretti, M. and Mastroddi, F. , Study of Reduced-Order Models for Gust-Response Analysis of Flexible Wings, *Journal of of Aircraft*, Vol. 41, No. 2, pp. 304-313, 2004.

[8] Lane, F., System Mode Shapes in the Flutter of Compressor Blade Rows, *Journal of the Aeronautical Sciences*, Vol. 23, No. 1 (1956), pp. 54-66.

[9] Kaza, K.R. and Kielb, R.E., Flutter and Response of a Mistuned Cascade in Incompressible Flow, *AIAA Journal*, Vol. 20, No. 8 (August 1982), pp. 1120-1127.

[10] He, Z., Epureanu, B.I. and Pierre, C. , Parametric Study of the Aeroelastic Response of Mistuned Bladed Disks, *Journal of Computer and Structures*, Vol. 85, pp. 852-867, February 2007

[11] Theodorsen, T., General Theory of Aerodynamic Instability and the Mechanism of Flutter, NACA Report 496, 1935.

[12] Greenberg, J.M., Airfoil in Sinusoidal Motion in a Pulsating Stream, NACA TN-1326, 1947.

[13] Bakhle, M.A., Reddy, T.S.R. and Keith, T.G., Time Domain Flutter Analysis of Cascades using Full-Potential Solver, *AIAA Paper* 1990-984, 1990.

[14] Whitehead, D.S. and Nagashima, T., Linearized Supersonic Unsteady Flow in Cascade, *ARC R&M* 3811, London, 1978.

[15] Buffum, D.H. and Fleeter, S., Aerodynamic of a Linear Oscillating Casacade, NASA TM 103250, August 1990.

[16] Buffum, D.H. and Boldman, D.R., Unsteady Aerodynamics of an Oscillating Cascade in a Compressible Flow Field, NASA TM 100219, September 1987.

[17] Jones, W.P. and Moore, J.A., Aerodynamic Theory for a Cascade of Oscillating Airfoils in Compressible Subsonic Flow, *AIAA Journal* 14-5, May 1976.

[18] Mendelson, A. and Carrol, R.W., Lift and Moment Equations for Oscillating Airfoils in an Infinite Unstaggered Cascade, NACA TN 3263, October 1954.

[19] Henderson, R.E. and Daneshyar, H., Theoretical Analysis of Fluctuating Lift on the Rotor of an Axial Turbomachine, *ARC R&M* 3684, London, 1972

[20] Adamczyk, J.J. and Goldstein, M. E., Unsteady Flow in a Supersonic Cascade with Subsonic Leading Edge Locus, *AIAA Journal*, Vol. 16, No. 12 (1978), pp. 1248-1254.

[21] Morino, L., Mastroddi, F., De Troia, R., Ghiringhelli, G.L. and Mantegazza, P., Matrix Fraction Approach for Finite-State Aerodynamic Modeling, *AIAA Journal*, Vol. 33, No. 4, pp. 703-711.